TECHNICAL RESEARCH REPORT

UNIVERSITY OF MARYLAND COLLEGE PARK 1856

SYSTEMS RESEARCH CENTER

VE RI TAS HARVARD

Supported by the National Science Foundation Engineering Research Center Program (NSFD CD 8803012), Industry and the University

The Workspace of Three-Degree-of-Freedom, Four-Jointed Spherical Wrist Mechanisms

by C.C. Lin and L.W. Tsai

TR 90-57

The Workspace of Three-Degree-of-Freedom, Four-Jointed Spherical Wrist Mechanisms

Chen-Chou Lin, Research Asistant
and
Lung-Wen Tsai, Professor

Department of Mechanical Engineering
and
Systems Research Center

The University of Maryland
College Park, MD 20742

August 29, 1990

ABSTRACT

In this paper, orientational workspace of three-degree-of-freedom, four-jointed spherical wrist mechanisms have been investigated. We have derived the workspace boundary equations via both geometric consideration and Jacobian analysis. It is shown that for the first type wrist mechanisms with links 2 and 3 coupled, the workspace boundary consists of circles centered at fixed axis of rotation; while for the second type mechanisms with links 1 and 2 coupled, the boundary consists of two branches of curves. The workspace is divided by inner and outer boundaries into regions of accessibility zero, two and four. The criteria for full workspace design as well as for maximum four-root region have been established.

1 Introduction

Recently, Lin and Tsai [6] developed an atlas of three-DOF (degree-of-freedom) bevel-gear-type wrist mechanisms. It was found that a three-DOF wrist mechanism can have more than three articulation points. Figure 1 shows three types of three-DOF, four-jointed wrist mechanisms in which the motion of: (i) links 2 and 3 are coupled, (ii) links 1 and 2 are coupled, and (iii) links 3 and 4 are coupled. In this paper, the workspace associated with type (i) and (ii) mechanisms will be studied. However, we shall not discuss type (iii) mechanism, because the end-effector can not possess an independent motion about the last joint axis. Motion such as drilling is not possible for such a wrist mechanism.

The workspace of a manipulator, as defined by Gupta and Roth [2], is the aggregate of all possible positions of a point attached to the free end of the manipulator. This definition of workspace is usually referred to as the reachable workspace. For orientational structures, the workspace can be defined in a similar manner, that is, the aggregate of all possible orientations of a frame attached to the end-effector of a manipulator. The orientation of a rigid body can be represented in many ways, such as Euler angles, roll-pitch-yaw angles, Euler parameters (unit quaternion), Rodrigues parameters, etc. Each representation has its advantages and disadvantages. If the approach vector $\vec{a}$ of an end-effector is coaxial with the last joint axis of a spherical wrist, then the orientation of the end-effector can be described by the direction of the last joint axis plus a rotation about it. Since the contribution to the workspace due to the last joint motion is always a constant, 2π, the workspace can be represented in a two dimensional space. Specifically, the spherical surface area swept by a point located on the last joint axis and one unit length away from the wrist center can be used to describe the workspace.

Workspace of three-jointed wrist mechanisms has been investigated by many researchers [3,5,8,9,10,11]. Some significant results have been derived from the application of Grashof-type conditions on spherical four-bar linkages. Gupta [3] derived general equations for the design of three-jointed spherical wrist mechanisms including non-zero twist angle of the gripper mount. It was concluded that maximal workspace can be obtained when the twist angle of the first two links is equal to $\pi/2$ and the joint axes intersect at a common point. Although the workspace associated with three-jointed wrist mechanisms has been studied extensively, the problem associated with three-DOF, four-jointed wrist mechanisms is completely new, and is the subject of this study.

2 Three-jointed wrist mechanisms

In what follows, it is assumed that (i) the joint axes intersect at a common point O called the wrist center, (ii) the twist angles of moving links (except the gripper mount) can not be zero or π, (iii) the twist angle of the gripper mount is zero, and (iv) mechanical interference will not be considered.

We shall use the D-H (Denavit-Hartenberg) parameters [1] and 3×3 rotation matrices for the analysis. Figure 2 shows a general three-DOF, three-jointed spherical wrist mechanism. The origin of each coordinate system is located at the wrist center. However, they have been sketched away from the wrist center for the reason of clarity. The $(XYZ)_0$ coordinate system is fixed to the base link with the X_0-axis pointing out of the paper. The other link coordinate systems are defined according to the D-H convention. We have chosen the stretched out, joint axes coplanar configuration of the mechanism as the reference position, and define all the positive X-axes to be pointing out of the paper. The joint angle θ_i is the angle measured from X_{i-1} to X_i-axis about the positive Z_{i-1}-axis. The directions of the Z-axes are chosen so that all the twist angles are less than π. The twist angle α_i is the angle measured from Z_{i-1} to Z_i-axis about the positive X_i-axis. The end-effector coordinate system can be chosen arbitrarily as long as the approach vector $\vec{a}$ is in line with the last joint axis.

Under the condition of zero twist angle between the last joint axis and the Z-axis of the hand coordinate system, we may use a more direct method to determine the workspace. Figure 3 shows that the end point P of a unit vector along the last joint axis will trace over a unit sphere. Let $W_k(P)$ be the workspace of the end point P with respect to a frame fixed in the kth link. Then, the workspace $W_{k-1}(P)$ can be obtained by revolving $W_k(P)$ about Z_{k-1} axis as suggested by Gupta and Roth [2]. In the three-jointed case, $W_1(P)$ is a circle whose radius is equal to $sin(\alpha_2)$. The workspace $W_0(P)$ is obtained by revolving the circle $W_1(P)$ about Z_0-axis and, therefore, is a partial spherical surface area $\mathcal{A}$. This area is continuous and axisymmetric with respect to the first axis of rotation $\vec{Z}_0$. There are two voids, V_1 and V_2, which are the aggregate of all unreachable orientations by the wrist mechanism. The boundaries, B_1 and B_2, are two circles centered at Z_0-axis, whose radii depend on the twist angles α_1 and α_2. Figure 3 shows that the radii of B_1 and B_2 are equal to $sin(\alpha_1 - \alpha_2)$ and $sin(\alpha_1 + \alpha_2)$, respectively. From the above analysis we can easily determine the orientational workspace, i.e. the shape of the area $\mathcal{A}$.

We may ask ourselves the following question. What are the twist angles required to produce a full orientational workspace, i.e. no voids on the sphere? The necessary and sufficient condition is that the radii of B_1 and B_2 are both equal to zero, that is,

$$s(\alpha_1 - \alpha_2) = 0 \tag{1.a}$$

and

$$s(\alpha_1 + \alpha_2) = 0 \tag{1.b}$$

where s denotes the sine function and, in what follows, we shall use c to denote the cosine function.

The only solution for the above equations is $\alpha_1 = \alpha_2 = \pi/2$. This result is identical to the result obtained by Gupta [3], but the approach is simpler.

As another example, assume that only the front void V_2 is to be eliminated, then Eq.(1.b) yields $\alpha_1 + \alpha_2 = \pi$. The twist angles, $\alpha_1 = \pi/3$ and $\alpha_2 = 2\pi/3$, of Cincinnati-Milacron 3-Roll wrist satisfy this condition. This design allows all the three joints to have full rotation without mechanical interference.

The boundaries separating $\mathcal{A}$ and the two voids can also be derived by the Jacobian analysis [4]. It can be proved that, the accessibility for any point inside the workspace $\mathcal{A}$ is two, which means there are two inverse solutions corresponding to each given end-effector orientation. The accessibility for any point inside the void is zero. We may consider the boundary as a transition region separating two areas of different accessibility. The accessibility on the boundaries is one. A special case is when the boundary lies on the fixed axis of rotation $\vec{Z}_0$, which results in an infinite accessibility.

3 Three-DOF, four-jointed mechanisms with links 2 and 3 coupled

Figure 1(a) shows a three-DOF, four-jointed wrist mechanism. The mechanism contains three input links labeled as 1, 5 and 6, and four joint axes labeled as a, b, c, and d. The bevel gears attached to links 1 and 3 are used for coupling the relative motion of link 2 with respect to link 1 to that of link 3 with respect to link 2. All the other bevel gears are used for power transmission. Overall, this mechanism contains nine links, eight revolute joints, and five gear pairs. The four joint axes, a, b, c, and d, intersect at a common point. Hence, the end-effector, link 4, possesses a spherical motion with three degrees of freedom. Figure 4 shows a similar mechanism with all the driving and driven gears removed for the convenience of discussion. In what follows, we shall choose the gear ratio for coupling the motion of links 2 and 3 to be one.

3.1 Workspace analysis

For the mechanism shown in Fig. 4, links 1, 2, and 3 form a one-DOF spherical planetary gear train, and $W_1(P)$ is a trajectory generated by the planetary gear train. The analysis of such trajectory has been studied extensively by Lin and Tsai [7]. The trajectory $W_1(P)$ traced by the end point of a unit vector $\vec{P}$ along the Z_3-axis and expressed in the $(XYZ)_1$ frame can be written as [7]

$$^1\vec{P} = \begin{bmatrix} c\theta_2 s\theta_3 s\alpha_3 + s\theta_2 c\theta_3 c\alpha_2 s\alpha_3 + s\theta_2 s\alpha_2 c\alpha_3 \\ s\theta_2 s\theta_3 s\alpha_3 - c\theta_2 c\theta_3 c\alpha_2 s\alpha_3 - c\theta_2 s\alpha_2 c\alpha_3 \\ -c\theta_3 s\alpha_2 s\alpha_3 + c\alpha_2 c\alpha_3 \end{bmatrix} \tag{2}$$

where $\theta_3 = \theta_2 + \theta_p$, and where θ_p is a phase angle.

Note that we have used a leading superscript to indicate the coordinate system in which the vector is expressed. A vector without a leading superscript indicates the vector is expressed in the base coordinate system $(XYZ)_0$.

In Fig. 4, we have chosen $\alpha_1 = \pi/2$, $\alpha_2 = \alpha_3 = \pi/3$, and $\theta_p = 0$ for the purpose of demonstration. The spatial drawing of $W_1(P)$ is shown in Fig. 5(a), and its Y_1Z_1 projection is shown in Fig. 5(b). The workspace $W_0(P)$ can be obtained by revolving $W_1(P)$ about the Z_0-axis.

Similar to three-jointed case, workspace $\mathcal{A}$ has two voids V_1 and V_2, and two circular boundaries B_1 and B_2 separating the voids and the workspace as shown in Fig. 5(b). However, the workspace $\mathcal{A}$ is further divided into two regions of different accessibility by an inner (circular) boundary B_3. In Fig. 5(b), let a point P be located in the region between B_1 and B_3. Then, revolving the trajectory about the Y_1-axis will sweep point P four times per revolution. Hence the area between B_1 and B_3 has an accessibility of four. Similarly, the region between B_2 and B_3 has an accessibility of two.

In general, when $\theta_p = 0$ and the twist angles α_1, α_2 and α_3 are arbitrary, the coordinates of the unit position vector $\vec{P}$, defined along the Z_3-axis and expressed in the $(XYZ)_0$ system, are given by

$$\vec{P} = \begin{bmatrix} x \\ y \\ z \end{bmatrix} = \begin{bmatrix} c\theta_1 & -s\theta_1 c\alpha_1 & s\theta_1 s\alpha_1 \\ s\theta_1 & c\theta_1 c\alpha_1 & -c\theta_1 s\alpha_1 \\ 0 & s\alpha_1 & c\alpha_1 \end{bmatrix} \begin{bmatrix} c\theta_2 s\theta_3 s\alpha_3 + s\theta_2 c\theta_3 c\alpha_2 s\alpha_3 + s\theta_2 s\alpha_2 c\alpha_3 \\ s\theta_2 s\theta_3 s\alpha_3 - c\theta_2 c\theta_3 c\alpha_2 s\alpha_3 - c\theta_2 s\alpha_2 c\alpha_3 \\ -c\theta_3 s\alpha_2 s\alpha_3 + c\alpha_2 c\alpha_3 \end{bmatrix} \tag{3}$$

where $\theta_3 = \theta_2 + \theta_p$.

The z-component of $\vec{P}$ is independent of θ_1, and its extreme values can be derived by setting its first derivative to zero, i.e.

$$\begin{aligned}\frac{dz}{d\theta_2} &= s\theta_2[2c\theta_2 s\alpha_3 s\alpha_1(1+c\alpha_2)+s\alpha_2 s(\alpha_1+\alpha_3)] \\ &= 0 \end{aligned} \tag{4}$$

Hence, the extreme values of z occur at:

$$\theta_2 = cos^{-1}\left(-\frac{s\alpha_2 s(\alpha_1+\alpha_3)}{2s\alpha_1 s\alpha_3\,(1+c\alpha_2)}\right), \tag{5.a}$$

$$\theta_2 = 0, \tag{5.b}$$

and

$$\theta_2 = \pi. \tag{5.c}$$

Equation (5.a) will not have real solutions if the absolute value in the argument of the arc cosine function is greater than one. Substituting the values of θ_2 from Eqs. (5.a), (5.b), and (5.c) into the third equation of Eq. (3), yields

$$z_a = s\alpha_1 s\alpha_3 + c\alpha_1 c\alpha_2 c\alpha_3 + \frac{s^2(\alpha_1+\alpha_3)(1-c\alpha_2)}{4s\alpha_1 s\alpha_3}, \tag{6.a}$$

$$z_b = c(\alpha_1+\alpha_2+\alpha_3), \tag{6.b}$$

and

$$z_c = c(\alpha_1-\alpha_2+\alpha_3), \tag{6.c}$$

respectively. Since $W_0(P)$ is obtained by revolving $W_1(P)$ about the Z_0-axis, the boundaries B_i of $W_0(P)$ depend on the extreme values of z. The radius of the circular boundary B_1 is the shortest distance between point a and Z_0-axis, which is

$$R_{B_1} = \sqrt{1-z_a^2} \tag{7.a}$$

Note that for $\theta_p = 0$, then $\theta_3 = \theta_2$ and the z-coordinate is a function of $\cos\theta_2$ only. Hence the two solutions of θ_2 given by Eq. (5.a) yield two points with the same

z-coordinate. The solutions of θ_2 given by Eqs. (5.b) and (5.c) yield points b and c. The coordinates of points b and c can be derived by substituting Eqs. (5.b) and (5.c) into Eq. (3), respectively. Therefore, the radii of B_2 and B_3 are given by:

$$R_{B_2} = \sqrt{1 - z_b^2} = |s(\alpha_1 + \alpha_2 + \alpha_3)| \tag{7.b}$$

$$R_{B_3} = \sqrt{1 - z_c^2} = |s(\alpha_1 - \alpha_2 + \alpha_3)| \tag{7.c}$$

If the phase angle $\theta_p \neq 0$, the trajectory shown in Fig. 5(a) will be rotated an angle $-\theta_p$ about the Z_1-axis. For $\theta_p = \pi/2$, the $Y_1 Z_1$ projection of the resulting trajectory is shown in Fig. 5(c). Revolving the trajectory about the Z_0-axis (Y_1 axis), results in a workspace $W_0(P)$ with four circular boundaries. The two outer boundaries B_1 and B_2 separate the workspace $\mathcal{A}$ and the voids, and the two inner boundaries B_3 and B_4 divide the workspace $\mathcal{A}$ into three regions, two regions with an accessibility of two and one region with an accessibility of four. The radii of B_1 through B_4 can be derived by finding points a', b', c', and d' with extreme z-coordinates. Equating the first derivative of z with respect to θ_2 to zero, we obtain

$$\begin{aligned} \frac{dz}{d\theta_2} &= s(2\theta_2 + \theta_p) s\alpha_1 s\alpha_3 (1 + c\alpha_2) + s\alpha_2 [s(\theta_2 + \theta_p) c\alpha_1 s\alpha_3 + s\theta_2 s\alpha_1 c\alpha_3] \\ &= 0 \end{aligned} \tag{8}$$

Equation (8) yields four solutions of θ_2 in the range of $-\pi < \theta_2 \leq \pi$. The solutions, $\tilde{\theta}_2$, of Eq. (8) define the positions of extreme points. Substituting $\tilde{\theta}_2$ and θ_p into Eq. (3), yields

$$\begin{aligned} z_i = {} & s\alpha_1 [s\tilde{\theta}_{2_i} s(\tilde{\theta}_{2_i} + \theta_p) s\alpha_3 - c\tilde{\theta}_{2_i} c(\tilde{\theta}_{2_i} + \theta_p) c\alpha_2 s\alpha_3 - c\tilde{\theta}_{2_i} s\alpha_2 c\alpha_3] \\ & + c\alpha_1 [c\alpha_2 c\alpha_3 - c(\tilde{\theta}_{2_i} + \theta_p) s\alpha_2 s\alpha_3] \end{aligned} \tag{9}$$

The radii of the circular boundaries are:

$$R_{B_i} = \sqrt{1 - z_i^2}, \qquad i = 1, 2, 3, 4. \tag{10}$$

3.2 Kinematic synthesis

In the synthesis of four-jointed spherical wrist mechanisms with links 2 and 3 coupled, it is desirable to have the workspace as well as the four-root region as large as possible. The advantage of four-roots over two-roots is that a mechanism with four roots has more choices of postures to orient the end-effector.

The workspace is determined by three parameters, α_1, α_2 and α_3. Its circular boundaries, B_i, are related to the extreme values of z given by Eqs. (6.a)-(6.c), or Eq. (9). Hence, if $\theta_p = 0$, then given the radii of the boundaries R_{B_i}, the twist angles α_1, α_2, and α_3 can be obtained by solving Eqs. (6.a) through (6.c) simultaneously. Figure 5(b) gives us some insight about the workspace limitation.

Now suppose a full workspace is desired. What are the twist angles? A full workspace has no voids. Therefore, the trajectory has to pass through the $z_0 = \pm 1$ points. It has been shown [7] that the trajectory intersects the $Y_1 Z_1$ plane at three points: b, c, and d, where b and c are the points having extreme z_1 coordinates, and point d is the node (double point) of the spherical limacon. The criterion for the spherical limacon to have a node is given by

$$\frac{\alpha_2}{2} < \alpha_3 < \pi - \frac{\alpha_2}{2} \tag{11}$$

The coordinates of the node, expressed in the $(XYZ)_1$ frame, are given by

$$^1\vec{P}_d = {}^1\vec{P}_{node} = \begin{bmatrix} 0 \\ s\alpha_3 \\ c\alpha_3 \end{bmatrix} \tag{12.a}$$

When $\theta_1 = \theta_p = 0$, it can be expressed in the $(XYZ)_0$ frame as

$$\vec{P}_d = \vec{P}_{node} = \begin{bmatrix} 0 \\ -s(\alpha_1 - \alpha_3) \\ c(\alpha_1 - \alpha_3) \end{bmatrix} \tag{12.b}$$

The coordinates of b and c, expressed in the $(XYZ)_1$ frame are given by:

$$^1\vec{P}_b = \begin{bmatrix} ^1x_b \\ ^1y_b \\ ^1z_b \end{bmatrix} = \begin{bmatrix} 0 \\ -s(\alpha_2 + \alpha_3) \\ c(\alpha_2 + \alpha_3) \end{bmatrix} \tag{13}$$

and

$$^1\vec{P}_c = \begin{bmatrix} ^1x_c \\ ^1y_c \\ ^1z_c \end{bmatrix} = \begin{bmatrix} 0 \\ s(\alpha_2 - \alpha_3) \\ c(\alpha_2 - \alpha_3) \end{bmatrix} \tag{14}$$

The angle ψ_z, measured from $\vec{P}_c$ to $\vec{P}_b$ in the clockwise direction, is given by

$$\psi_z = 2(\pi - \alpha_2) \tag{15}$$

There are three cases from which full workspace can be achieved:

Case (1): Z_0-axis passes through points b and c of the trajectory.

In this case, points b and c subtend the origin at an angle equal to π. Equating Eq. (15) to π yields

$$\alpha_2 = \pi/2 \tag{16.a}$$

Equating Eqs. (6.b) and (6.c) to -1 and +1, respectively, and eliminating α_2 from the two equations yields

$$\alpha_1 + \alpha_3 = \pi/2 \tag{16.b}$$

Case (2): Z_0 axis passes through points b and d of the trajectory.

In this case, points b and d subtend the origin at an angle equal to π. Taking the dot product of Eqs. (13), and (12.a) yields

$$^1\vec{P}_b \cdot {}^1\vec{P}_{node} = c(2\alpha_3 + \alpha_2) = -1.$$

Hence,

$$2\alpha_3 + \alpha_2 = \pi. \tag{17.a}$$

For the existence of a node, solving Eq. (17.a) for α_3 and then substituting it into Eq. (11), yields

$$\alpha_2 < \pi/2. \tag{17.b}$$

Equating the z-component of Eq. (12.b) to +1, yields

$$\alpha_1 = \alpha_3. \tag{17.c}$$

<u>Case(3): Z_0 axis passes through points c and d of the trajectory.</u>

In this case, points c and d subtend the origin at an angle equal to π. Taking the dot product of Eqs. (14), and (12.a) yields

$$^1\vec{P}_c \cdot \, ^1\vec{P}_{node} = c(2\alpha_3 - \alpha_2) = -1.$$

Hence,

$$2\alpha_3 - \alpha_2 = \pi. \tag{18.a}$$

For the existence of a node, solving Eq. (18.a) for α_3 and then substituting it into Eq. (11), yields

$$\alpha_2 < \pi/2. \tag{18.b}$$

Equating the z-component of Eq. (12.b) to +1, yield

$$\alpha_1 = \alpha_3 \tag{18.c}$$

Note that α_1, α_2 and α_3 can not be 0 or π, in which case the mechanism will degenerate and lose one degree of freedom.

Hence, if $\theta_p = 0$, Eqs. (16.a)-(16.b), or Eqs. (17.a)-(17.c), or Eqs. (18.a)-(18.c) are the necessary conditions for a mechanism to have full workspace. For examples, for case (1) $\alpha_1 = \pi/6$, $\alpha_2 = \pi/2$, and $\alpha_3 = \pi/3$ satisfy Eqs. (16.a) and (16.b); for case (2) $\alpha_1 = \pi/3$, $\alpha_2 = \pi/3$, and $\alpha_3 = \pi/3$ satisfy Eqs. (17.a) (17.b) and (17.b); and for case (3) $\alpha_1 = 2\pi/3$, $\alpha_2 = \pi/3$, and $\alpha_3 = 2\pi/3$, satisfy Eqs. (18.a) (18.b) and (18.b). Among the three cases, case (1) has an accessibility of two for the entire workspace while cases (2) and (3) contain a four-root region. To maximize the four-root region for case (2), Eqs. (7.b) or (7.c) can be used for the determination of the inner boundary B_{in}. If $R_{B_{in}} = 0$, then two extreme cases occur. One is the entire workspace is a two-root region, the other is a entire four-root region. Substituting $R_{B_3} = 0$ in Eq. (7.c), and solving it simultaneously with Eqs. (17.a) and (17.c), we obtain two sets of solutions. One is $\alpha_1 = \alpha_3 = \pi/4$, and $\alpha_2 = \pi/2$; and the other is $\alpha_1 = \alpha_3 = \pi/2$, and $\alpha_2 = 0$. Although the latter is the solution for a maximum four-root region, it results in a degenerate mechanism. Case (3) is actually the mirror image of case (2). Substituting $R_{B_2} = 0$ into Eq. (7.b), and solving it simultaneously with Eqs. (18.a) and (18.c), yields $\alpha_1 = \alpha_3 = \pi/2$, and $\alpha_2 = 0$ as the solution for an entire four-root workspace; and $\alpha_1 = \alpha_3 = 3\pi/4$, and $\alpha_2 = \pi/2$ for an entire two-root workspace.

If $\theta_p \neq 0$, the workspace is defined by four extreme points, namely, the z-coordinates of the centers of four circular boundaries, given by Eq. (9). The design is much more complicated than the $\theta_p = 0$ case.

3.3 Jacobian analysis

It is well-known that boundaries of workspace can be derived from Jacobian analysis. Jacobian curve (or surface) is defined as the space in which the rank of Jacobian matrix is lower than its order. When the determinant of Jacobian matrix becomes zero, there will be at least two equal roots of the characteristic polynomial [4], and the curves divide the wrokspace into regions of different accessibility. The angular velocity of the end effector, with respect to the $(XYZ)_0$ coordinate system and expressed in the $(XYZ)_1$, can be written as follows:

$$
\begin{aligned}
{}^1\vec{\omega}_4 &= \dot{\theta}_{10}\vec{Z}_0 + \dot{\theta}_{21}\vec{Z}_1 + \dot{\theta}_{32}\vec{Z}_2 + \dot{\theta}_{43}\vec{Z}_3 \\
&= \dot{\theta}_{10}\vec{Z}_0 + \dot{\theta}_{21}\vec{Z}_1 + n\dot{\theta}_{21}\vec{Z}_2 + \dot{\theta}_{43}\vec{Z}_3 \\
&= \begin{bmatrix} \vec{Z}_0 & \vec{Z}_1 + n\vec{Z}_2 & \vec{Z}_3 \end{bmatrix} \begin{bmatrix} \dot{\theta}_1 \\ \dot{\theta}_2 \\ \dot{\theta}_4 \end{bmatrix} \qquad (19)
\end{aligned}
$$

where $n = \frac{N_1}{N_3}$ is the gear ratio, and $\vec{Z}_i$ is a unit vector in the Z_i-axis direction. Expressing the vector $\vec{Z}_0$, $\vec{Z}_1 + n\vec{Z}_2$ and $\vec{Z}_3$ in the $(XYZ)_1$ coordinate system, the Jacobian matrix can be written as

$$
J = \begin{bmatrix} 0 & ns\theta_2 s\alpha_2 & c\theta_2 s\theta_3 s\alpha_3 + s\theta_2 c\theta_3 c\alpha_2 s\alpha_3 + s\theta_2 s\alpha_2 c\alpha_3 \\ s\alpha_1 & -nc\theta_2 s\alpha_2 & s\theta_2 s\theta_3 s\alpha_3 - c\theta_2 c\theta_3 c\alpha_2 s\alpha_3 - c\theta_2 s\alpha_2 c\alpha_3 \\ c\alpha_1 & 1 + nc\alpha_2 & -c\theta_3 s\alpha_2 s\alpha_3 + c\alpha_2 c\alpha_3 \end{bmatrix} \qquad (20)
$$

where $\theta_3 = n\theta_2 + \theta_p$.

The three column vectors in the Jacobian matrix are the instantaneous screw axes of the wrist mechanism. If the rank of the Jacobian matrix becomes less than three, the three instantaneous screw axes become coplanar. The solutions of $det(J) = 0$ define the singular conditions and Jacobian curves. When n is equal to one, then the singular condition can be written as.

$$
\begin{aligned}
det(J) &= s\alpha_1 s\alpha_3(1 + c\alpha_2)s(2\theta_2 + \theta_p) + s\alpha_2[s\alpha_1 c\alpha_3 s\theta_2 + c\alpha_1 s\alpha_3 s(\theta_2 + \theta_p)] \\
&= 0, \qquad (21)
\end{aligned}
$$

which is the same as Eq. (8). We have just shown that boundary curves can be obtained from either geometric consideration or Jacobian analysis.

4 Three-DOF, four-jointed mechanisms with links 1 and 2 coupled

Figure 1(b) shows a three-DOF, four-jointed wrist mechanism. Links 1, 5 and 7 are three input links. The bevel gears attached to links 0 and 2 are used to couple the relative motion of link 2 with respect to link 1 to that of link 1 with respect to link 0. All the other bevel gears are used for power transmission. The four joint axes, a, b, c, and d, intersect at a common point. Hence, the end-effector, link 4, possesses a spherical motion with three degrees of freedom. Figure 6 shows a similar mechanism with all the driving and driven gears removed from the mechanism. It can be clearly seen that links 0, 1, and 2 form a one-DOF spherical planetary gear train. In what follows, we shall choose the gear ratio for coupling the motion of links 1 and 2 to be one. Hence, the trajectory of a point on the third j oint axis is a spherical limacon.

4.1 Workspace analysis

The workspace analysis for four-jointed spherical wrist mechanisms with links 1 and 2 coupled is more involved, since the approach of revolving $W_1(P)$ about Z_0-axis can no longer be used. In this case, $W_2(P)$ is a circle which is centered about the third joint axis having its radius equal to $\sin(\alpha_3)$. And the workspace $W_0(P)$ is obtained by integrating $W_2(P)$ for every point Q on the spherical limacon traced by first two links. We shall first investigate the accessibility and boundaries of workspace from geometric consideration.

Figure 7(a) through 7(c) shows the spatial drawings of the workspace for this type of mechanisms. In Fig. 7(a), the twist angles are $\alpha_1 = \alpha_2 = \pi/2$, and $\alpha_3 = \pi/9$. Curve C is the spherical limacon traced by the end-point located on the third joint axis of link 2 and one unit away from the origin. The workspace $W_0(P)$ is obtained by sweeping $W_2(P)$ along C, which results in a figure-8 band on the sphere. Note that the spherical limacon C is the center-line of the band and the 'bandwidth' is $2\alpha_3$. The envelopes of all $W_2(P)$, B_1 and B_2, form the inner and outer boundaries of the workspace.

As shown in Fig. 7(a), the accessibility in the light-gray areas is two, because every point in these areas (except boundaries) are swept by $W_2(P)$ twice for each cycle of θ_1; and the accessibility in the dark-gray area is four, since the band overlaps itself in that area. The white areas are voids. For the example, Fig. 7(a) shows three voids: two of them are 'inside' and the third is 'outside' the limacon. We define the partial spherical surface within the figure-eight as the interior of the spherical limacon. The accessibility on the boundary is one, except for the portions enclosing the dark-gray area where the accessibility is three.

From the above geometric discussion, the boundary curves, B_1 and B_2, can be found analytically. In Fig. 7(a), let Q be an arbitrary point on the spherical limacon. Then, for $\theta_p = 0$, the position vector of point Q can be written as a function of the twist angles and the first joint angle as

$$\vec{Q} = \begin{bmatrix} c\theta_1 s\theta_1 s\alpha_2 + s\theta_1 c\theta_1 c\alpha_1 s\alpha_2 + s\theta_1 s\alpha_1 c\alpha_2 \\ s^2\theta_1 s\alpha_2 - c^2\theta_1 c\alpha_1 s\alpha_2 - c\theta_1 s\alpha_1 c\alpha_2 \\ -c\theta_1 s\alpha_1 s\alpha_2 + c\alpha_1 c\alpha_2 \end{bmatrix} \tag{22}$$

Corresponding to each point Q, there are two boundary points, P_1 and P_2. According to a property in spherical geometry, the arc $\widehat{QP_1}$ (or $\widehat{QP_2}$) along the great circle is normal to C and B_1 (or B_2). The vector $\vec{T}$ tangent to C at point Q can be obtained by differentiating Eq. (22) with respect to θ_1, that is,

$$\vec{T} = \begin{bmatrix} (1 + c\alpha_1)s\alpha_2 c2\theta_1 + s\alpha_1 c\alpha_2 c\theta_1 \\ (1 + c\alpha_1)s\alpha_2 s2\theta_1 + s\alpha_1 c\alpha_2 s\theta_1 \\ s\alpha_1 s\alpha_2 s\theta_1 \end{bmatrix}_Q \tag{23}$$

The vector tangent to the great arc $\widehat{P_1P_2}$ at Q is normal to both $\vec{Q}$ and $\vec{T}$, i.e.

$$\vec{N} = \vec{Q} \times \vec{T} \tag{24}$$

The position vectors of P_1 and P_2 are given by

$$\vec{P_1} = c\alpha_3\vec{Q} + \frac{s\alpha_3}{\|\vec{N}\|}\vec{N}, \tag{25}$$

and

$$\vec{P_2} = c\alpha_3\vec{Q} - \frac{s\alpha_3}{\|\vec{N}\|}\vec{N} \tag{26}$$

where $\|\vec{N}\|$ is the length of the vector $\vec{N}$.
Equations (25) and (26) provide the parametric forms of boundary curves.

As shown in Fig. 7(a), the shape of boundaries is closely related to that of the limacon and the twist angle α_3. If α_3 is small, there may be two voids inside the noded limacon, and the boundary curves B_1 and B_2 are parallel to the limacon C. In this case, the workspace forms a figure-eight band similar to the shape of the limacon. As α_3 increases, the inner voids become smaller and smaller, and finally disappear completely, leaving only an outer void. Figure 7(b) shows the case, $\alpha_3 = \pi/6$, for which the inner voids begin to disappear. If α_3 is further increased, till $\alpha_3 = \pi/2$, both inner and outer voids will completely disappear. As shown in Fig. 7(b), the workspace $W_0(P)$ can be thought of as the union of two bounded regions, S_1 and S_2. Each region is bounded by a curve, B_1 or B_2. The intersection of these two bounded regions forms a four-root region (dark-gray area). This approach of determining the accessibility of workspace only applies to situations where the spherical limacon has a node, and where there is no inner voids. It is also possible, however, that the outer void may disappear before the inner voids do. This situation usually occurs when α_1 is small. Figure 7(c) shows such an example.

Based on the above analysis, we conclude that the workspace can be found by plotting the boundary curves given by Eqs. (25) and (26) and then find the area bounded by these two curves. Figures 8(a)-(f) show the workspace of mechanisms with their first two twist angles taken from the spherical planetary gear trains shown in Figs. 4(a)-(f) in [7], and with $\alpha_3 = \pi/2$, respectively. (Note that α_2 and α_3 in Fig. 4 in [7] correspond to α_1 and α_2 in Fig. 8.) In Figs. 8(a)-(d), there are two two-root regions separated by one four-root region; while in Figs. 8(e)-(f), there are two four-root regions separated by one two-root region. The difference is due to the criterion given by Eq. (11). The accessibility on boundary curves is three, except for the cusps and those points having extreme y-coordinates where the accessibility is two. An inspection of Figs. 8(a)-(f) reveals that the workspace is symmetric with respect to the XY-plane when $\alpha_2 = \pi/2$, and the four-root region increases as α_1 decreases.

Since the workspace is obtained by sweeping $W_2(P)$ along the limacon, some geometric properties of the boundaries can be stated as follows:

P1 Adding a phase angle θ_p has the effect of rotating the workspace about Z_0-axis an angle $-\theta_p$.

P2 When $\theta_p = 0$, the workspace is symmetric about the Y-Z plane.

P3 When $\alpha_2 = \pi/2$, the workspace is symmetric about the X-Y plane.

P4 Given α_1 and α_2, maximum workspace is achieved if $\alpha_3 = \pi/2$.

P5 Given α_1 and α_2, the workspace derived for $\alpha_3 = \alpha_0$ is the mirror image of the workspace derived for $\alpha_3 = \pi - \alpha_0$.

P6 The workspace may have both inner and outer voids if α_3 is too small.

4.2 Kinematic synthesis

In the previous section, we have known that the workspace can be obtained by sweeping $W_2(P)$ along a spherical limacon. To achieve full workspace, the twist angles should be properly chosen so that there are no inner and outer voids. In what follows, we shall limit the angle α_3 to be no larger than $\pi/2$, because of the geometric properties **P4** and **P5** stated in the previous section. The following objectives will be explored for the workspace synthesis of three-DOF, four-jointed spherical wrist mechanisms with links 1 and 2 coupled: (i) to establish design criteria for full workspace, and (ii) to maximize the four-root regions.

As shown in Fig. 7(a), inner voids will exist if the radius of $W_2(P)$ is too small to cover the interior of the spherical limacon. Therefore, to eliminate inner voids, the twist angle α_3 should be greater than $\psi_x/2$, i.e.,

$$\alpha_3 \geq \psi_x/2 \tag{27}$$

where ψ_x is the angle between $\vec{Q}_{x_{max}}$ and $\vec{Q}_{x_{min}}$, and where $Q_{x_{max}}$ and $Q_{x_{min}}$ are the points on the spherical limacon having maximum and minimum x-coordinates, respectively. The locations of $\vec{Q}_{x_{max}}$ and $\vec{Q}_{x_{min}}$ can be found by substituting

$$\theta_1 = cos^{-1}\left(\frac{-u_1 \pm \sqrt{u_1^2 + 8u_0^2}}{4u_0}\right) \tag{28}$$

into Eq. (22), where $u_0 = s\alpha_2 + c\alpha_1 s\alpha_2$, and $u_1 = s\alpha_1 c\alpha_2$. Although there can be two $\vec{Q}'_{x_{max}}s$, and $\vec{Q}'_{x_{min}}s$ only the greater one is considered. Equation (27) can also be written in terms of the x-coordinates of $Q_{x_{max}}$ as follows:

$$\alpha_3 \geq sin^{-1}(x_{max}) \tag{29}$$

Similarly, to eliminate outer void only, it is necessary that

$$\alpha_3 \geq \pi - \psi_z/2, \tag{30}$$

where ψ_z is the angle measure from $\vec{Q}_{z_{max}}$ to $\vec{Q}_{z_{min}}$ in the clockwise direction, and is given by

$$\psi_z = 2(\pi - \alpha_1).$$

Hence, Eq. (30) can also be written as

$$\alpha_3 \geq \alpha_1 \tag{31}$$

Therefore, we conclude that in order to achieve a full workspace design, the necessary and sufficient condition is

$$\alpha_3 \geq Max(\alpha_1, sin^{-1} x_{max}) \tag{32}$$

For a given choice of α_1 and α_2, $\alpha_3 = \pi/2$ results in a largest workspace with no inner voids. Hence, by applying Eq. (31), we can conclude that a sufficient condition for full workspace design is

$$\alpha_3 = \pi/2 \text{ and } \alpha_1 \leq \pi/2 \tag{33}$$

In general, ψ_x is a function of α_1 and α_2. Hence, for each α_2, we can use Eqs. (22) and (28) to compute ψ_x as a function of α_1. Figure 9 shows five such curves for $\alpha_2 = 50, 60, 70, 80, 90$ degrees, respectively. Also shown in Fig. 9 is the curve $\alpha_3 = \alpha_1$. The intersection of $\alpha_3 \geq \alpha_1$ and $\alpha_3 \geq \psi_x/2$ is the solution space satisfying full workspace consideration.

From previous analysis, it is known that a four-root region is the intersection of two bounded regions S_1 and S_2. Hence, a large $W_2(P)$ is a necessary condition for achieving large area of overlapping. In addition, when the limacon is symmetric with respect to the XY plane, it will also produce larger overlapping area. We conclude it is necessary that $\alpha_2 = \alpha_3 = \pi/2$ in order to achieve a full workspace with maximum four-root region. With $\alpha_2 = \alpha_3 = \pi/2$, the smaller the angle α_1 is, the larger the four-root region is achieved. If $\alpha_1 = 0$, $\alpha_2 = \alpha_3 = \pi/2$, the mechanism will have its entire spherical surface filled with four-root region. However, this results in a degenerated mechanism. The design shown in Fig. 8(d), ($\alpha_1 = \pi/3$, $\alpha_2 = \pi/2$,$\alpha_3 = \pi/2$), seems to be better than others. Its advantages are:

(i) It has a full workspace with large four-root region.

(ii) The inner boundary curves are symmetric about the X-Y, X-Z, and Y-Z planes. Hence, its mechanical performance in each quadrant is equal.

(iii) The undesirable singular point at $z = -1$ is avoided.

4.3 Jacobian analysis

The angular velocity of the end effector in a four-jointed wrist mechanism with links 1 and 2 coupled can be written as follows:

$$\begin{aligned} {}^1\vec{\omega}_4 &= \dot{\theta}_{10}\vec{Z}_0 + \dot{\theta}_{21}\vec{Z}_1 + \dot{\theta}_{32}\vec{Z}_2 + \dot{\theta}_{43}\vec{Z}_3 \\ &= \dot{\theta}_{10}\vec{Z}_0 + n\dot{\theta}_{10}\vec{Z}_1 + \dot{\theta}_{32}\vec{Z}_2 + \dot{\theta}_{43}\vec{Z}_3 \\ &= \begin{bmatrix} \vec{Z}_0 + n\vec{Z}_1 & \vec{Z}_2 & \vec{Z}_3 \end{bmatrix} \begin{bmatrix} \dot{\theta}_1 \\ \dot{\theta}_3 \\ \dot{\theta}_4 \end{bmatrix} \end{aligned} \tag{34}$$

where n is the gear ratio $(\frac{N_0}{N_2})$.

The Jacobian matrix can be expressed in the $(XYZ)_1$ coordinate system as

$$J = \begin{bmatrix} 0 & s\theta_2 s\alpha_2 & c\theta_2 s\theta_3 s\alpha_3 + s\theta_2 c\theta_3 c\alpha_2 s\alpha_3 + s\theta_2 s\alpha_2 c\alpha_3 \\ s\alpha_1 & -c\theta_2 s\alpha_2 & s\theta_2 s\theta_3 s\alpha_3 - c\theta_2 c\theta_3 c\alpha_2 s\alpha_3 - c\theta_2 s\alpha_2 c\alpha_3 \\ c\alpha_1 + n & c\alpha_2 & -c\theta_3 s\alpha_2 s\alpha_3 + c\alpha_2 c\alpha_3 \end{bmatrix} \tag{35}$$

where $\theta_2 = n\theta_1 + \theta_p$.

The column vectors in the Jacobian matrix represent three instantaneous screw axes for the motion of the wrist mechanism. Unlike those mechanisms with links 2 and 3 coupled, all the instantaneous screw axes change their directions with respect to the base link as the mechanism rotates. This property provides an advantage for this type of wrist mechanisms. That is, singular points at $z = \pm 1$ can be avoided. For other three-DOF wrist mechanisms, when the last joint axis is in line with the fixed axis, the mechanism will lose one degree of freedom, which severely limits the manipulability in the frontal working zone. Actually, singular points still exist for this type of mechanisms, they are those points having extreme y-coordinates as shown in Fig. 8. At those points, all four joint axes become coplanar, and the end-effector can not make an instantaneous rotation about the direction perpendicular to that plane.

When the gear ratio $n = 1$, the singular condition is

$$\begin{aligned} det(J) &= s\alpha_3[(c\alpha_1 s\alpha_2 + s\alpha_2 + s\alpha_1 c\alpha_2 c\theta_2)s\theta_3 + s\alpha_1 s\theta_2 c\theta_3] \\ &= 0 \end{aligned} \tag{36}$$

Equation (36) has infinite many solutions. Solving Eq. (36) for θ_3, we obtain

$$\theta_3 = \tan^{-1}\left(-\frac{s\alpha_1 s\theta_2}{c\alpha_1 s\alpha_2 + s\alpha_2 + s\alpha_1 c\alpha_2 c\theta_2}\right) \tag{37}$$

Equation (37) explicitly expresses the relation between θ_3 and θ_2 when the mechanism is at a singular point. Parametric equations for the singular points can be obtained by substituting Eq. (37) into (3), with $\theta_2 = \theta_1 + \theta_p$. The equations are very tedious and are not presented here. The Jacobian curves are actually the boundary curves, B_1 and B_2, derived in Eqs. (25) and (26).

5 Summary

We have investigated the orientational workspace associated with two types of three-DOF, four-jointed spherical wrist mechanisms. An important step in the workspace analysis is the derivation of the geometric properties associated with spherical planetary gear trains. It has been shown elsewhere that the trajectory traced by a one-DOF, spherical planetary gear train is a spherical limacon. In this paper, we have shown that it is preferable for a spherical limacon to have a node and to be symmetrical in order to maximize the large four-root region.

For three-DOF, four-jointed wrist mechanisms with links 2 and 3 coupled, we have used the approach of revolving $W_1(P)$ about the fixed joint axis. The approach has been successfully applied to both analysis and synthesis problems. The relationship between the radii of boundary curves and the twist angles, and the criterion for full workspace design have been derived.

For three-DOF, four-jointed wrist mechanisms with links 1 and 2 coupled, the criteria for full workspace design and maximum four-root region have been established. This type of mechanisms has the advantage of avoiding its singular points to occur at $z = \pm 1$ locations. Therefore, the manipulability in the frontal working zone can be improved. Parametric equations for the workspace boundaries have been derived from both geometric consideration and Jacobian analysis. It is found that the boundaries consist of two branches of curves.

The advantage of four-jointed mechanisms is that the number of inverse solutions is greater than that of three-jointed mechanisms. Hence, without adding extra degrees of freedom, they can offer more choices of postures to orient the end-effector. Although singularities can not be fully eliminated, they can be located in a more desirable area by choosing the design parameters properly.

Acknowledgement

This work was supported in part by the U.S. Department of Energy under Grant DEF05-88ER13977 and in part by the NSF Engineering Research Centers Program, NSFD CDR 8803012. Such support does not constitute an endorsement by the supporting agencies of the views expressed in the paper.

References

[1] Denavit, J., and Hartenberg, R.S., 1955, "*A Kinematic Notation for Lower Pair Mechanisms Based on Matrices,*" ASME Journal of Applied Mechanics, Vol. 77, pp. 215-221.

[2] Gupta, K.C., and Roth, B., 1982, *"Design Considerations for Manipulator Workspace,"* ASME Journal of Mechanical Design, Vol. 104, pp 704-712.

[3] Gupta, K.C., 1986, *"Rotatability Considerations for Spherical Four-Bar Linkages With Applications to Robot Wrist Design,"* ASME Journal of Mechanisms, Transmissions, and Automation in Design, Vol 108, pp. 387-391.

[4] Kohli, D, and Hsu, M.S., 1987, *"The Jacobian Analysis of Workspace of Mechanical Manipulators,"* Mechanisms and Machine Theory, Vol. 22, pp. 265-275.

[5] Kumar, A., and Waldron, K.J., 1980, *"The Dexterous Workspace,"* ASME Paper No. 80-DET-108.

[6] Lin, C.C., and Tsai, L.W., 1989, *"The Development of an Atlas of Bevel-Gear-Type Spherical Wrist Mechanisms,"* Proceedings of First National Conference on Applied Mechanisms and Robotics, Paper No. 89-AMR-2A-3, Cincinnati, OH., Nov. 5-8, 1989.

[7] Lin, C.C., and Tsai, L.W., 1990, *"The Trajectory Analysis of Spherical Planetary Gear Trains,"* to be submitted for Publication in ASME Journal of Mechanical Design and for presentation at The 1991 ASME Design Automation Conference.

[8] Paul, R.P., and Stevenson, C.N., 1983, *"Kinematics of Robot Wrists,"* International Journal of Robotics Research, Vol. 2, No. 1, pp. 31-38.

[9] Roth, B., 1975, *"Performance Evaluation of Manipulators From Kinematic Viewpoint,"* NBS Special Publication- Performance Evaluation of Programmable Robots and Manipulators, pp. 39-61.

[10] Stackhouse, T., 1979, *"A New Concept in Wrist Flexibility,"* Proceedings of the 9th International Symposium on Industrial Robots, Washington, DC, pp. 589-599.

[11] Vijaykumar, R., Tsai, M.J., and Waldron, K.J., 1985, *"Geometric Optimization of Manipulator Structures for Working Volume and Dexterity,"* Proceedings of the IEEE International Conference on Robotics and Automation, St. Louis, pp. 228-236.

CAPTIONS

Figure 1. Three-Degree-of-Freedom, Four-Jointed Bevel-Gear-Type Spherical Wrist Mechanisms

Figure 2. An Open-Loop, Three-Jointed Spherical Wrist Mechanism.

Figure 3. Orientational Workspace of A Three-Jointed Spherical Wrist Mechanism.

Figure 4. A Four-Jointed Spherical Wrist Mechanism With Links 2 and 3 Coupled.

Figure 5(a). A Spherical Limacon with $\alpha_2 = \pi/3$ and $\alpha_3 = \pi/3$.

Figure 5(b). Workspace Generated By Revolving The Limacon About Z axis ($\theta_p = 0$).

Figure 5(c). Workspace Generated by Revolving The Limacon About Z axis ($\theta_p = \pi/2$).

Figure 6. A Four-Jointed Spherical Wrist Mechanism With Links 1 and 2 Coupled.

Figure 7. Workspace Generated by Sweeping $W_2(P)$ Along A Spherical Limacon ($\theta_p = 0$).

Figure 8. Bounadry Curves and Areas of Different Accessibility of Four-Jointed Spherical Wrist Mechanisms With Links 1 and 2 Coupled.

Figure 9. The Criteria for Full Workspace Design: $\alpha_3 > \alpha_1$ and $\alpha_3 > \frac{1}{2}\psi_x$

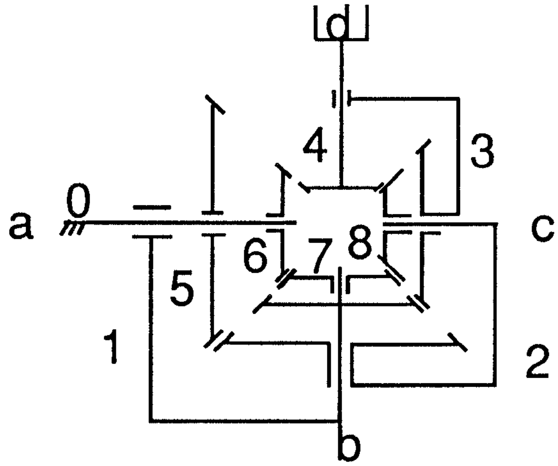

(a) links 2 & 3 coupled

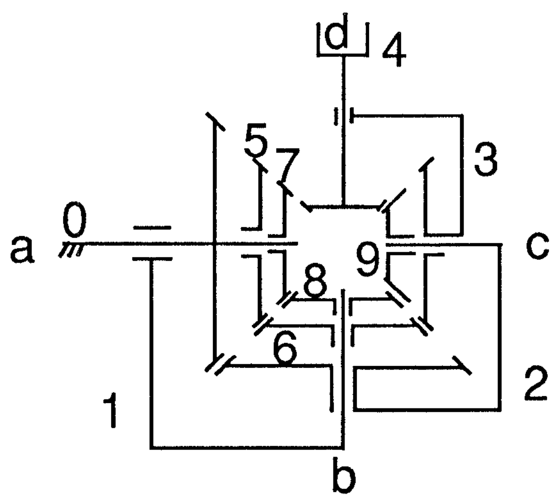

(b) links 1 & 2 coupled

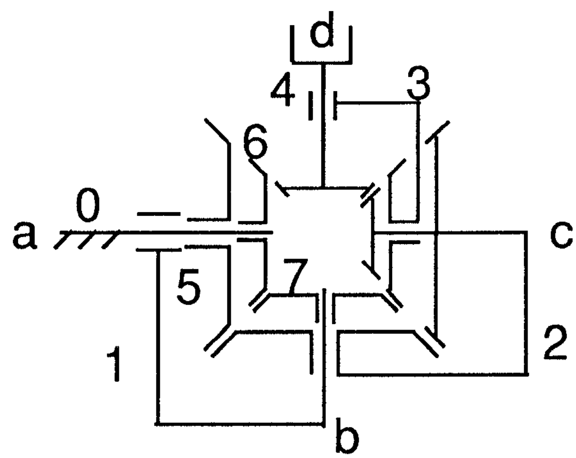

(c) links 3 & 4 coupled

Figure 1

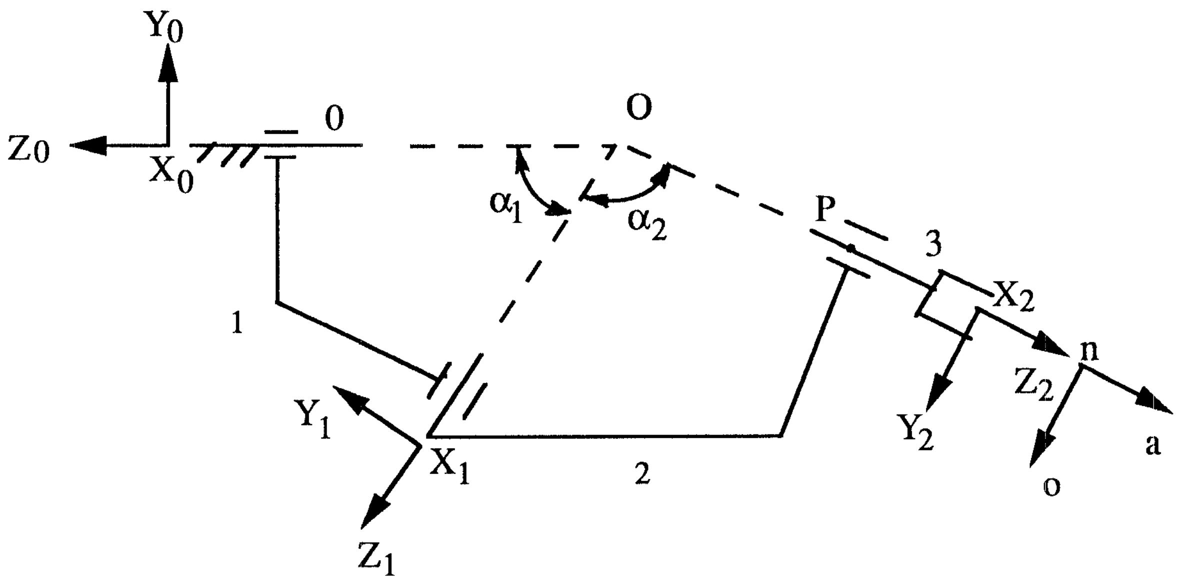

Figure 2

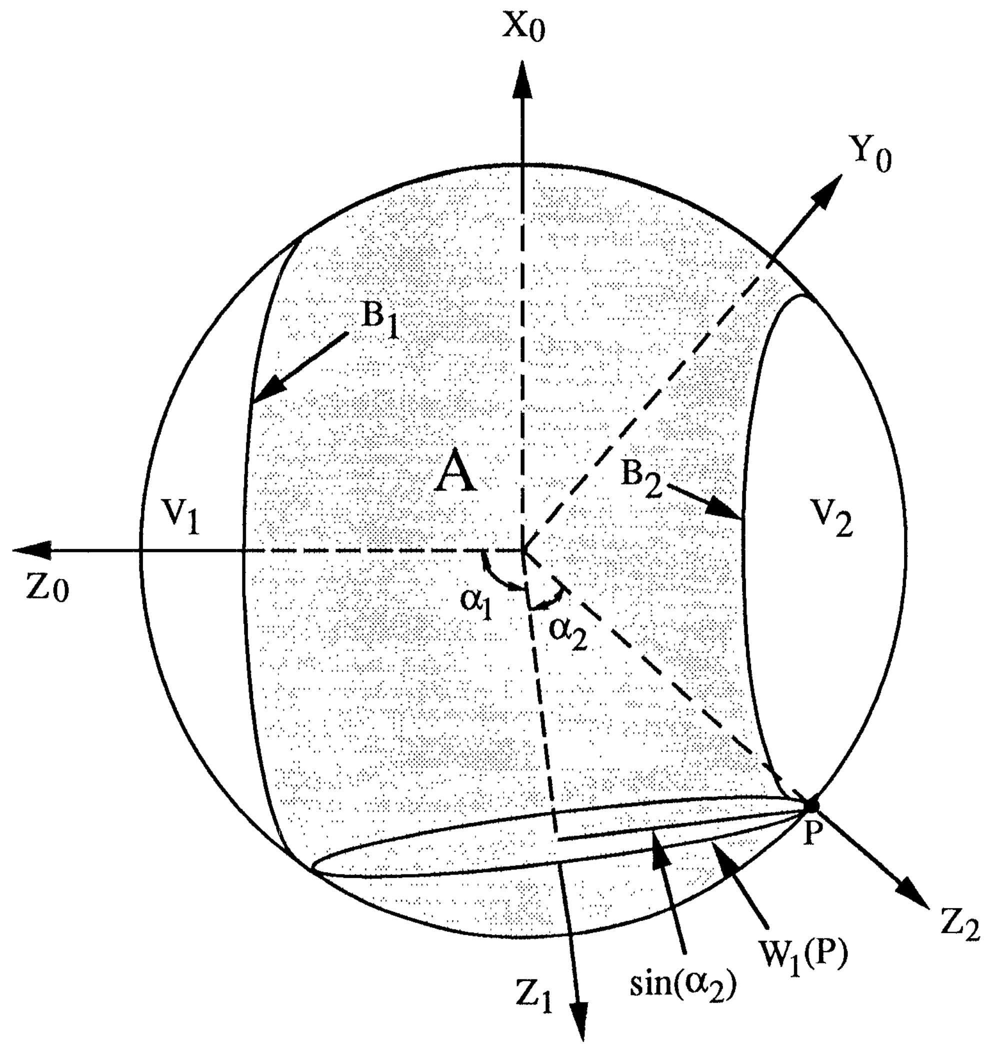

Figure 3

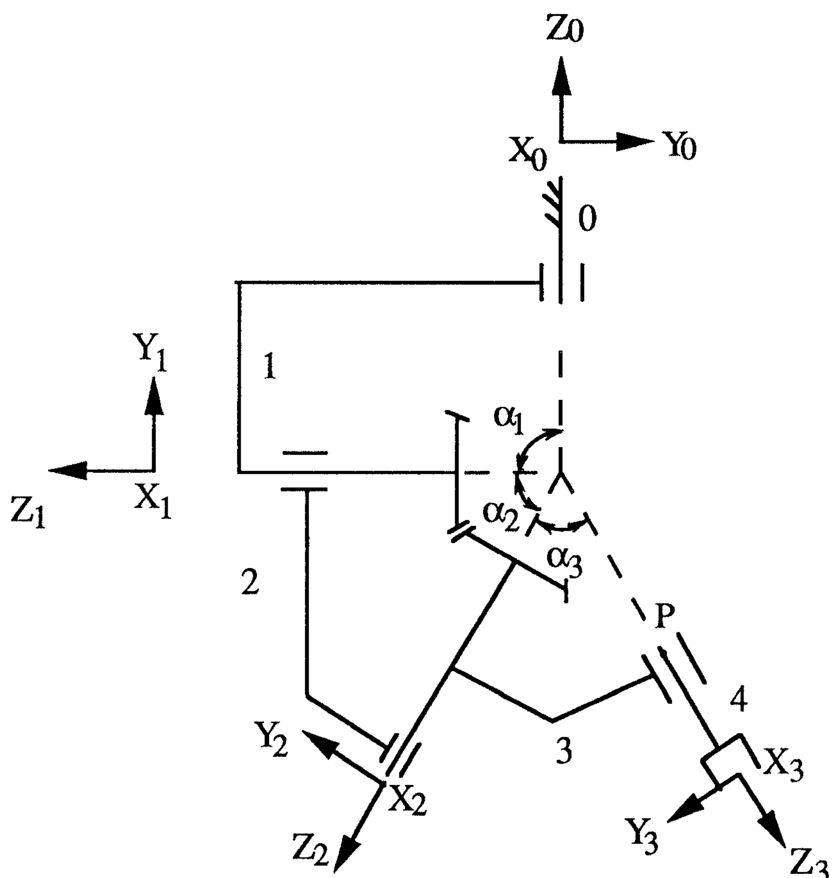

Figure 4

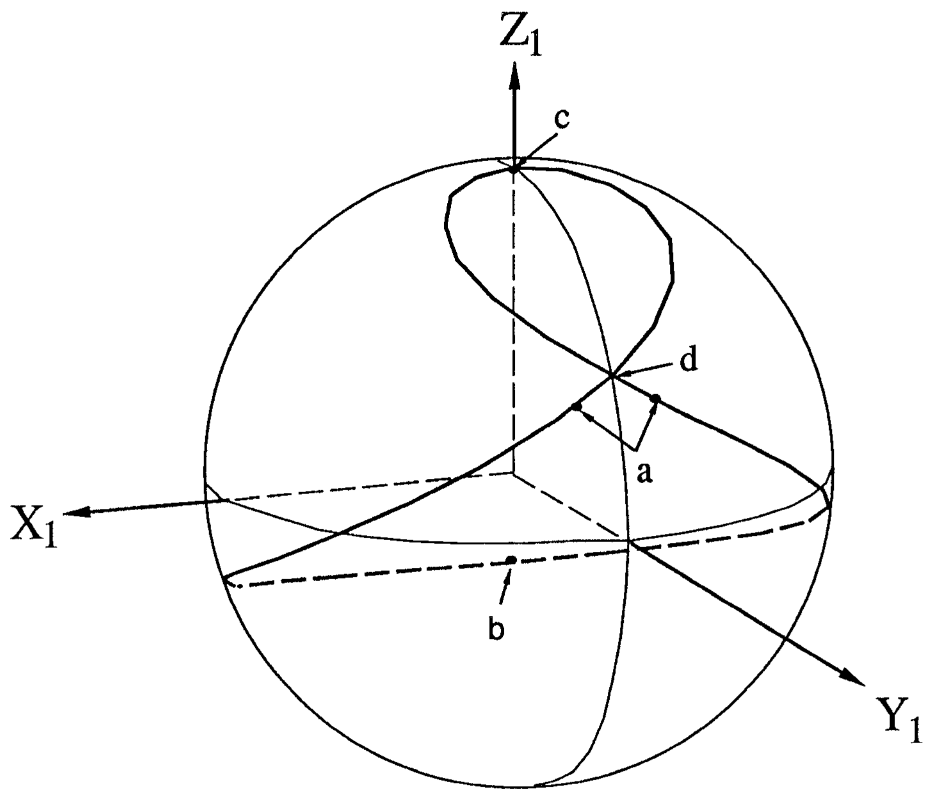

(a)

Figure 5

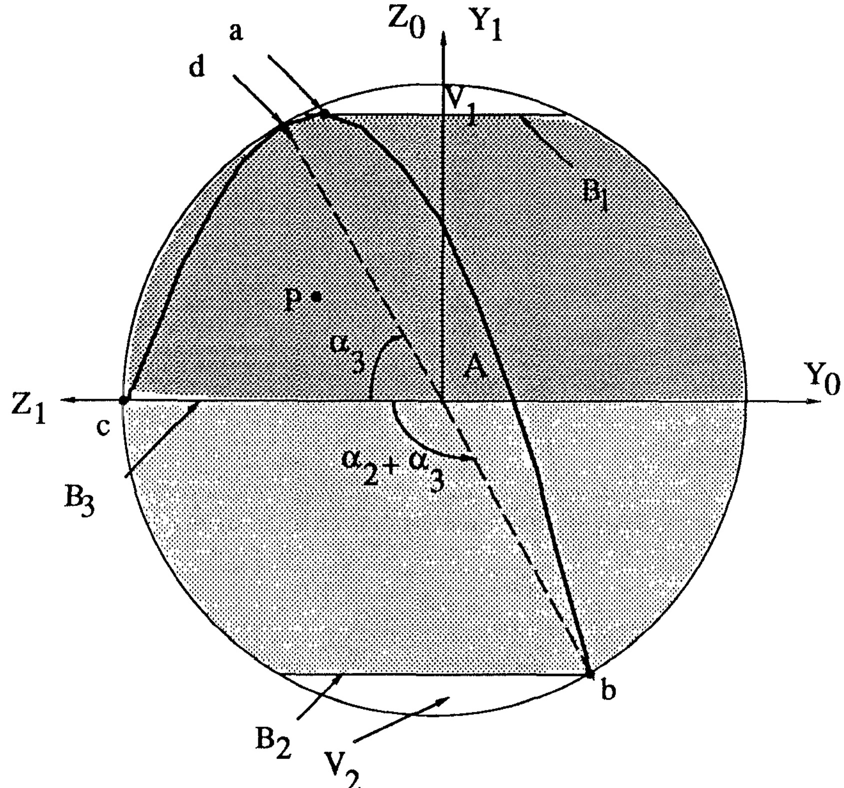

a
d
Z_0
Y_1
V_1
B_1
P
α_3
A
Y_0
Z_1
c
B_3
$\alpha_2+\alpha_3$
b
B_2
V_2

(b)

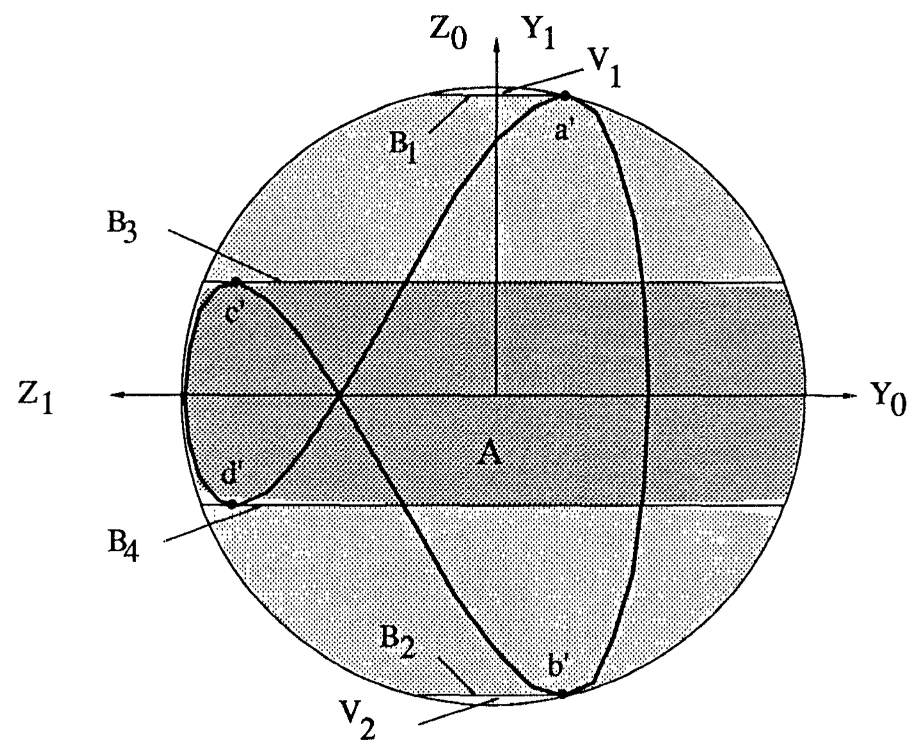

Z_0
Y_1
V_1
B_1
a'
B_3
c'
Z_1
Y_0
A
d'
B_4
B_2
b'
V_2

(c)

Figure 5

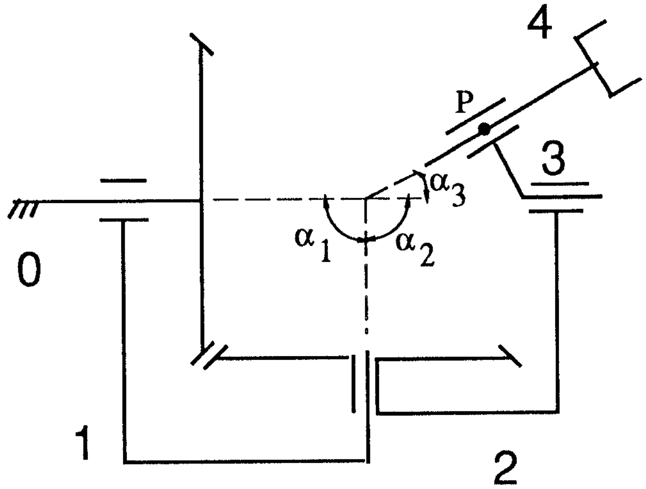

Figure 6

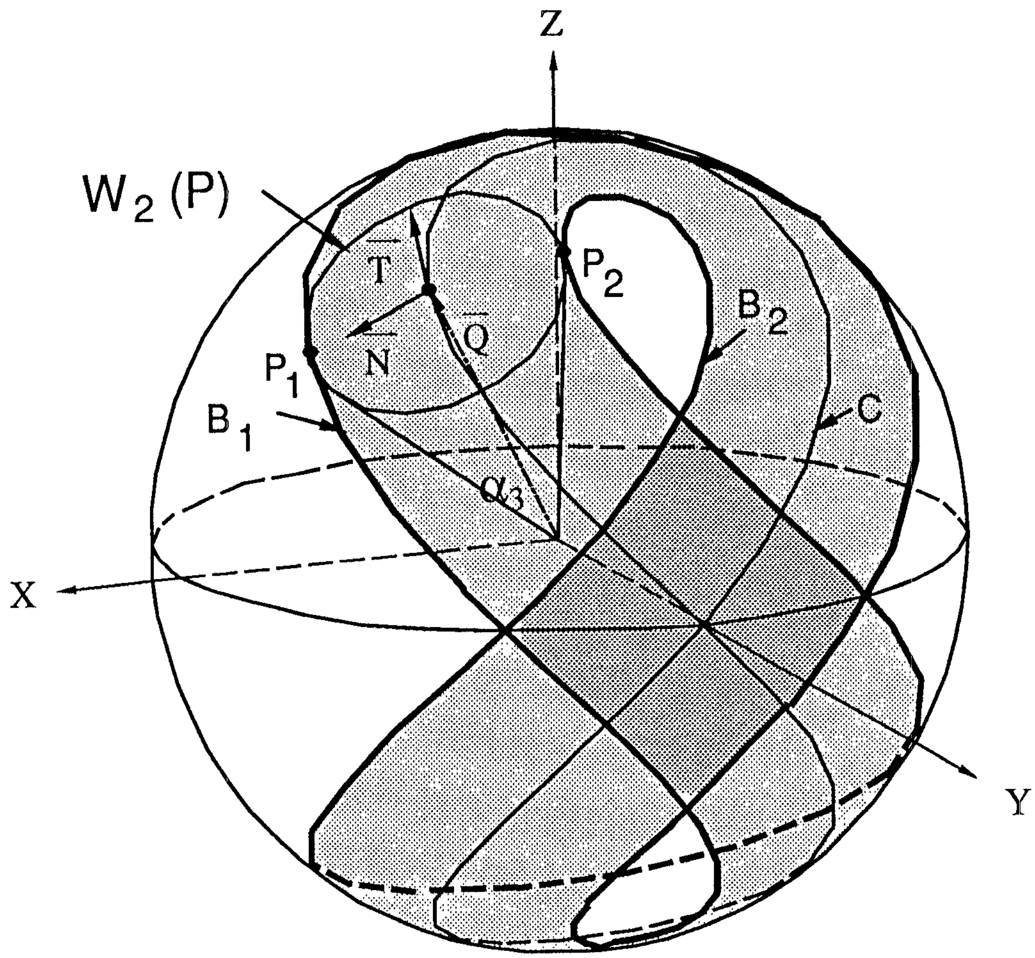

$\alpha_1 = \pi/2 \qquad \alpha_2 = \pi/2 \qquad \alpha_3 = \pi/9$

(a)

Figure 7

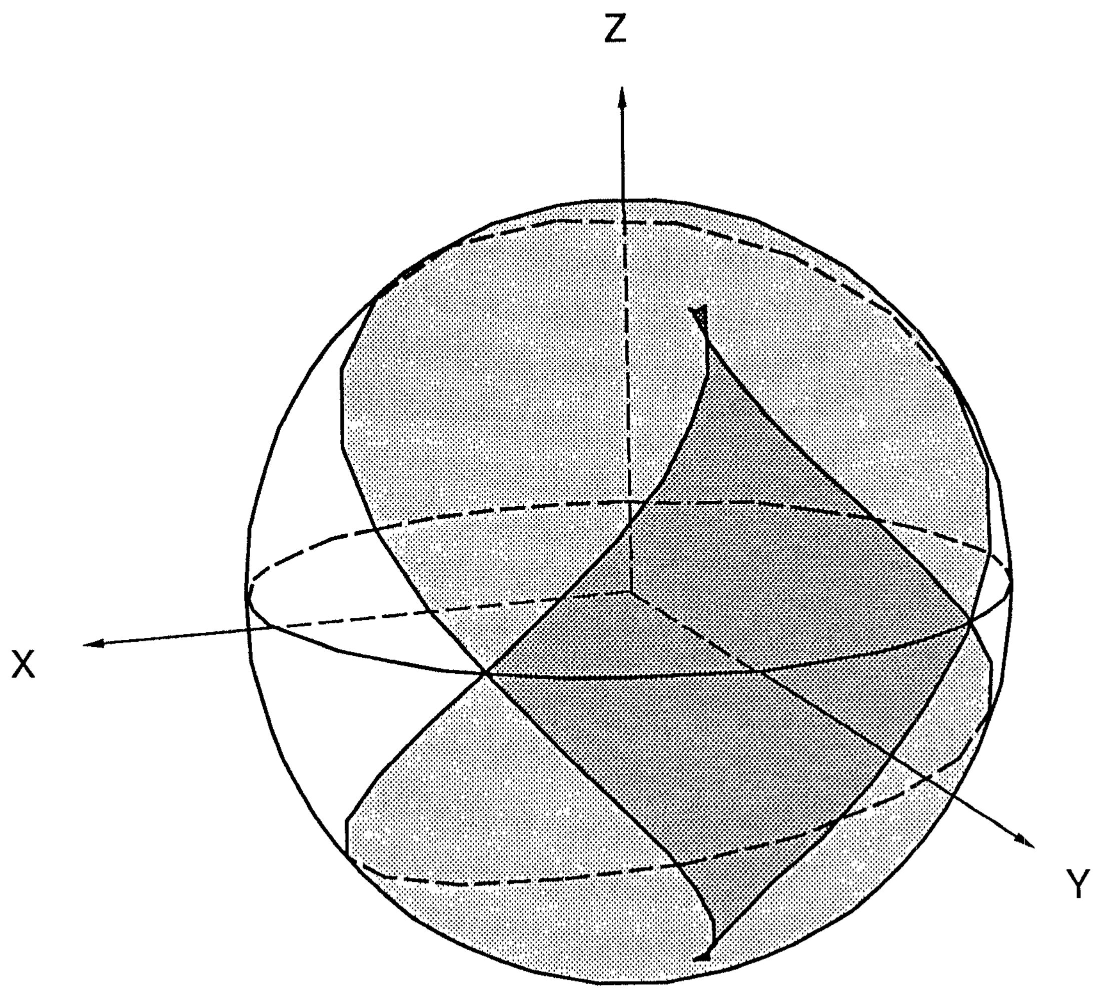

$\alpha_1 = \pi/2 \qquad \alpha_2 = \pi/2 \qquad \alpha_3 = \pi/6$

(b)

Figure 7

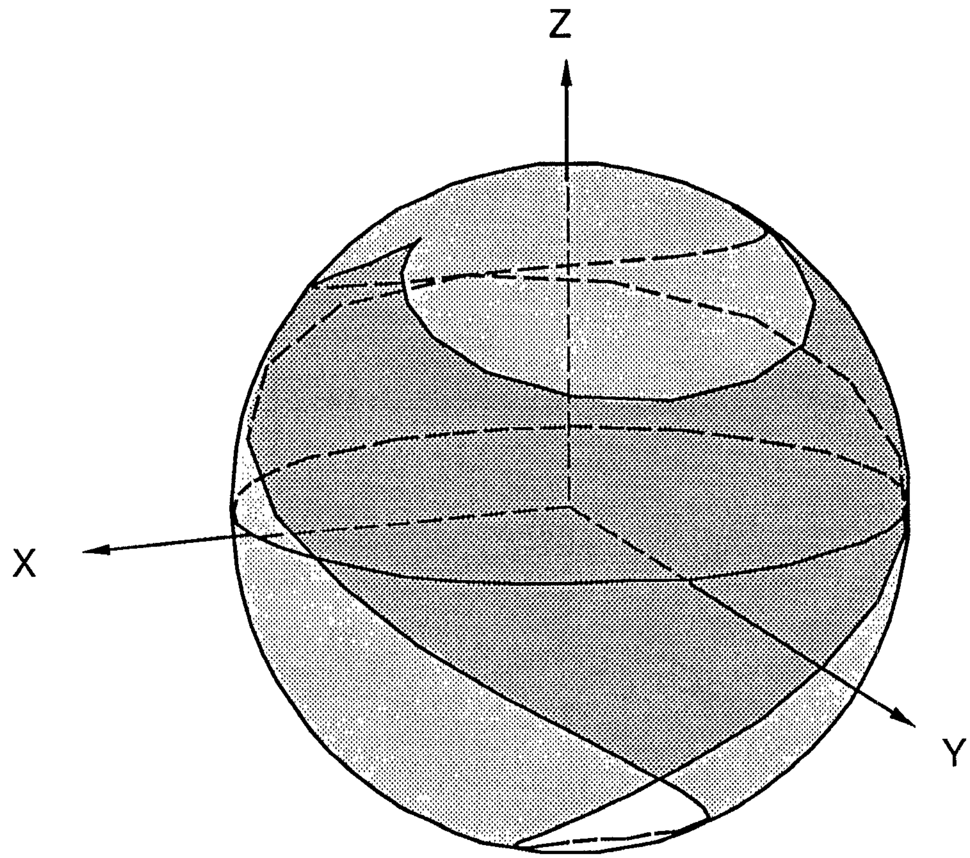

$\alpha_1 = \pi/3 \qquad \alpha_2 = \pi/3 \qquad \alpha_3 = \pi/3$

(c)

Figure 7

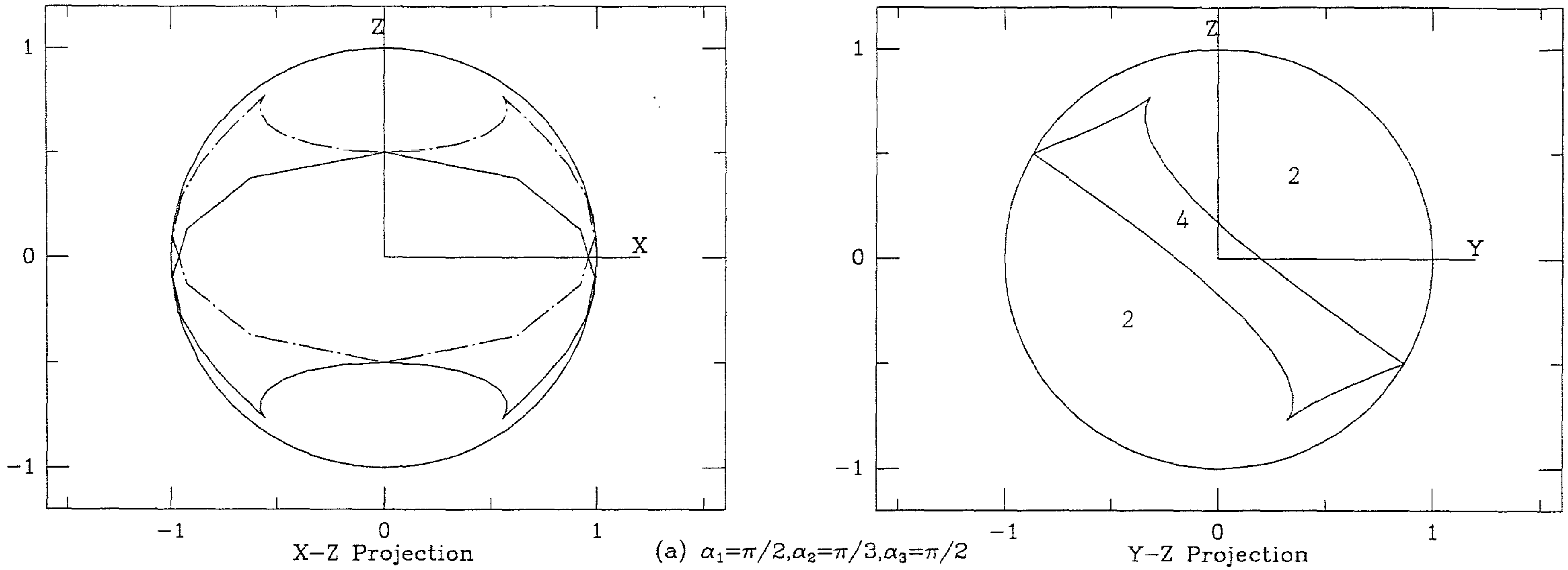

(a) $\alpha_1=\pi/2, \alpha_2=\pi/3, \alpha_3=\pi/2$

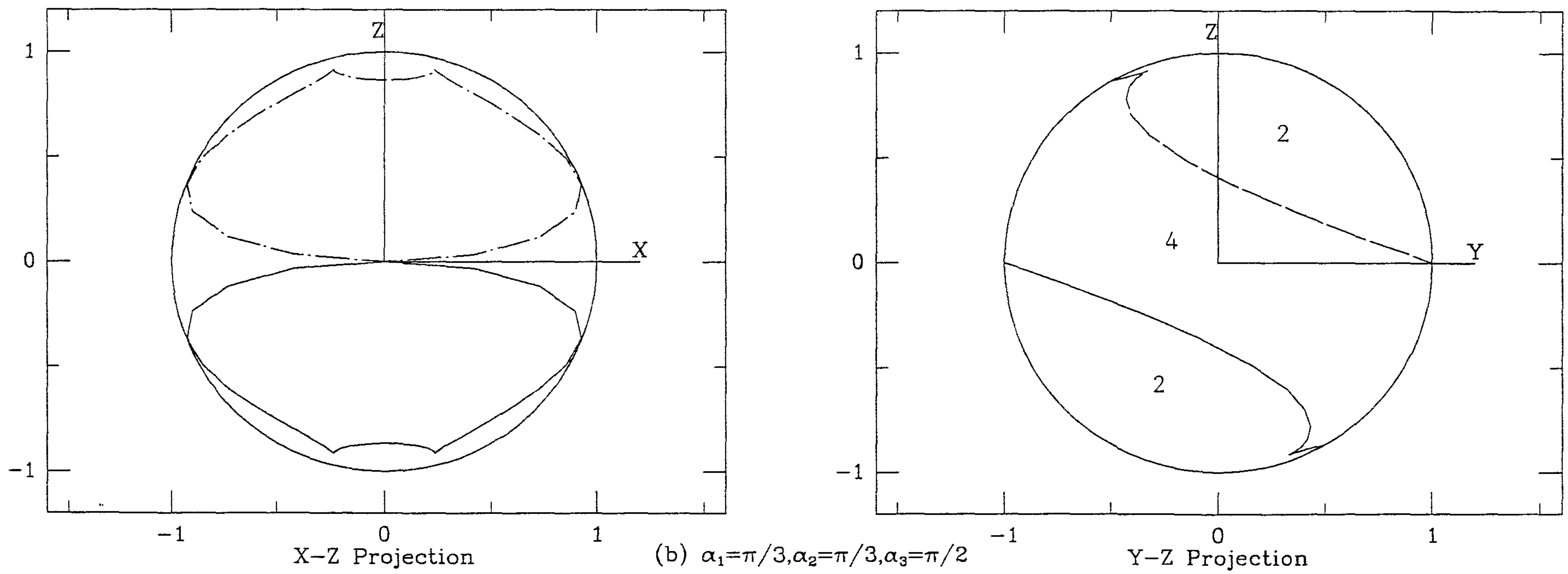

(b) $\alpha_1=\pi/3, \alpha_2=\pi/3, \alpha_3=\pi/2$

Figure 8

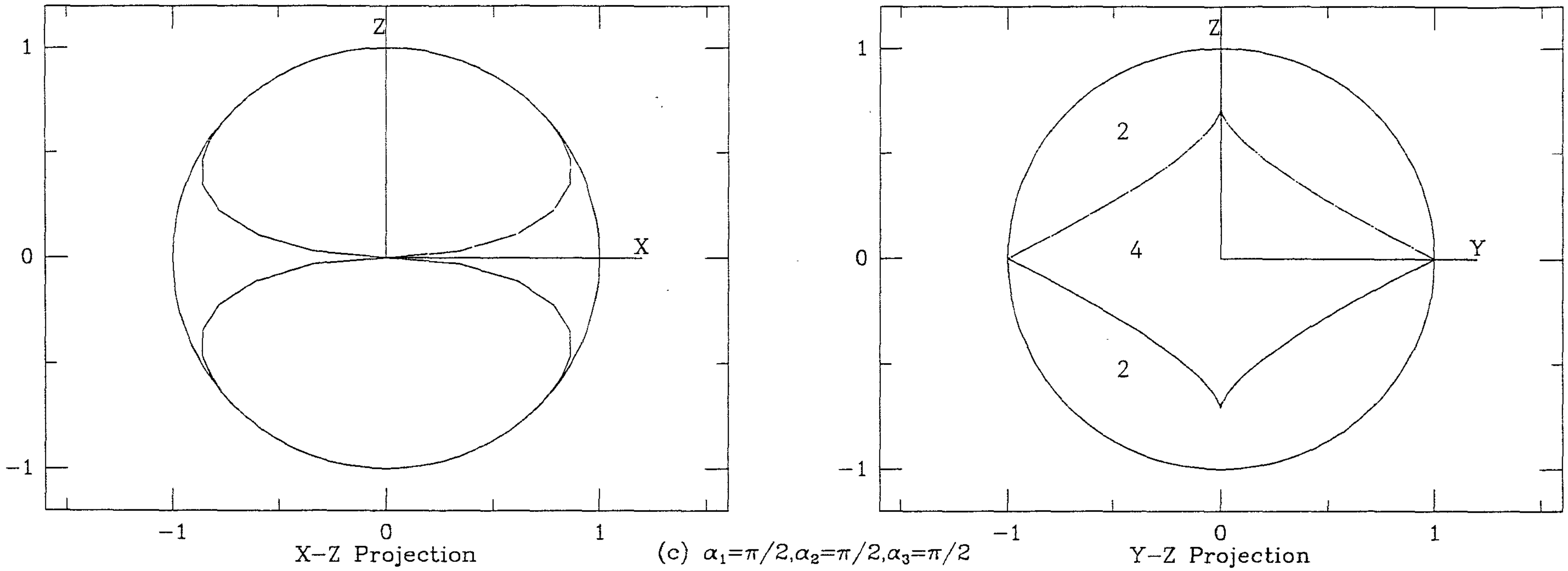

(c) $\alpha_1=\pi/2, \alpha_2=\pi/2, \alpha_3=\pi/2$

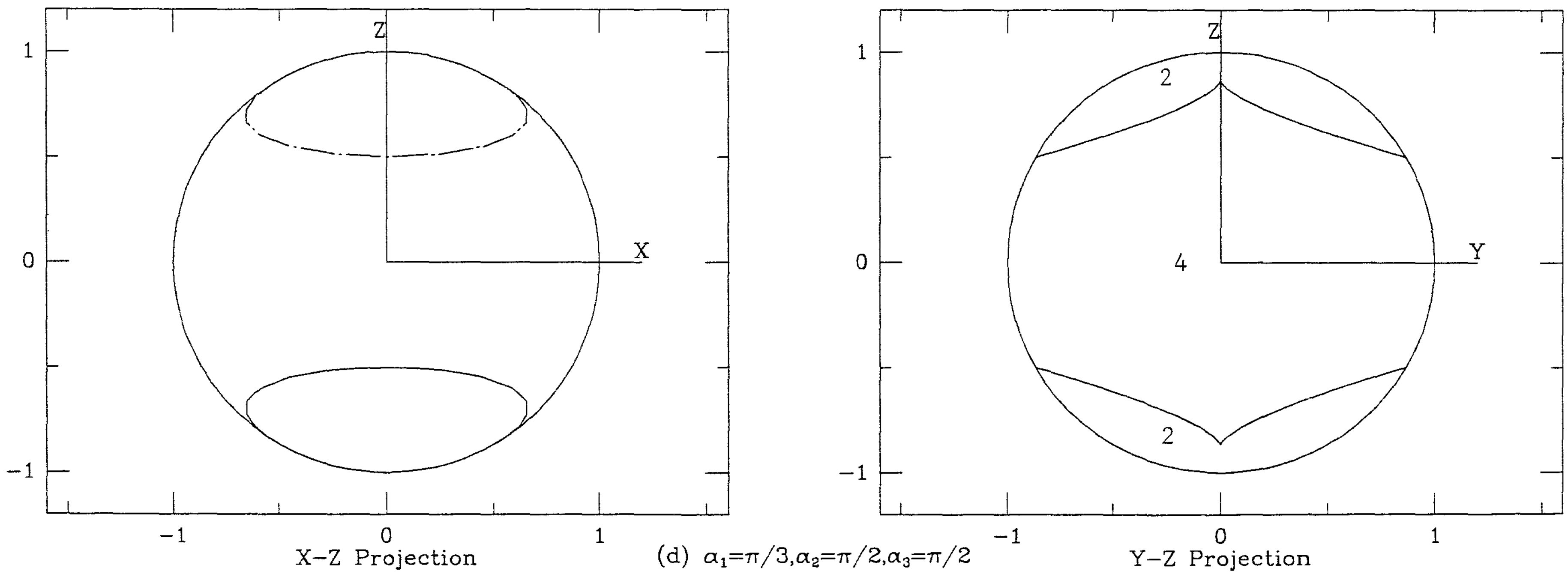

(d) $\alpha_1=\pi/3, \alpha_2=\pi/2, \alpha_3=\pi/2$

Figure 8 (Continued)

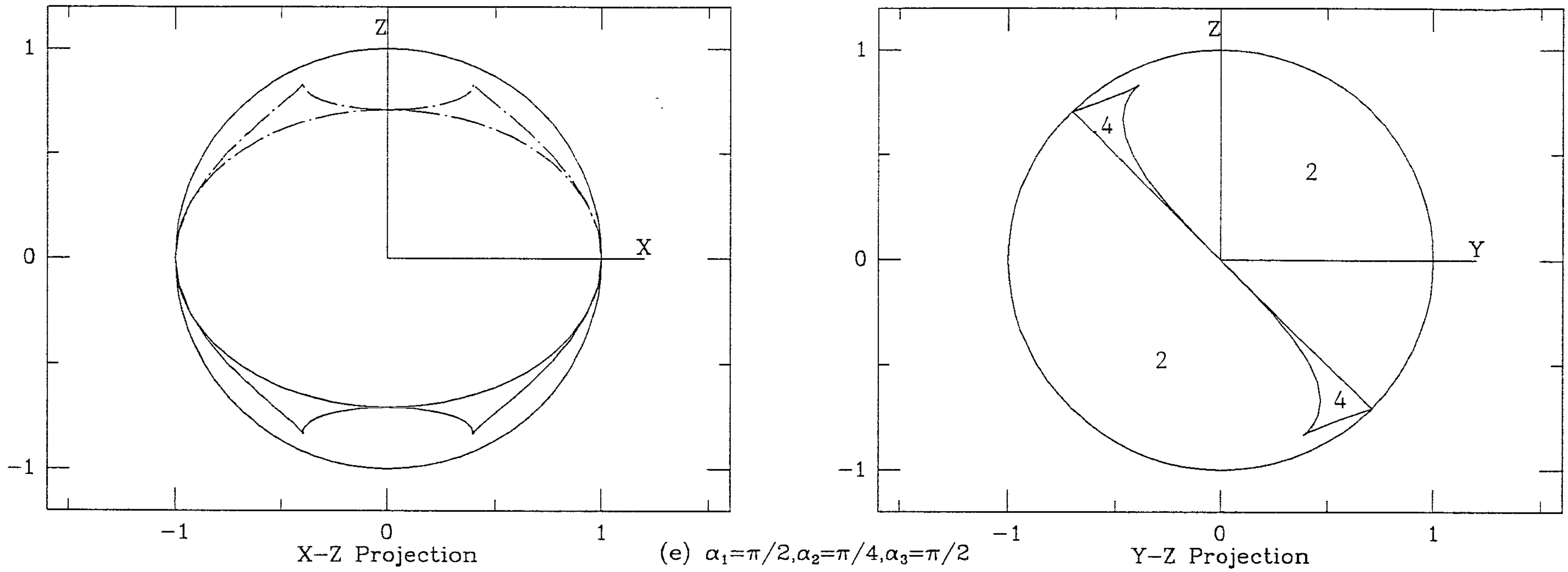

(e) $\alpha_1=\pi/2, \alpha_2=\pi/4, \alpha_3=\pi/2$

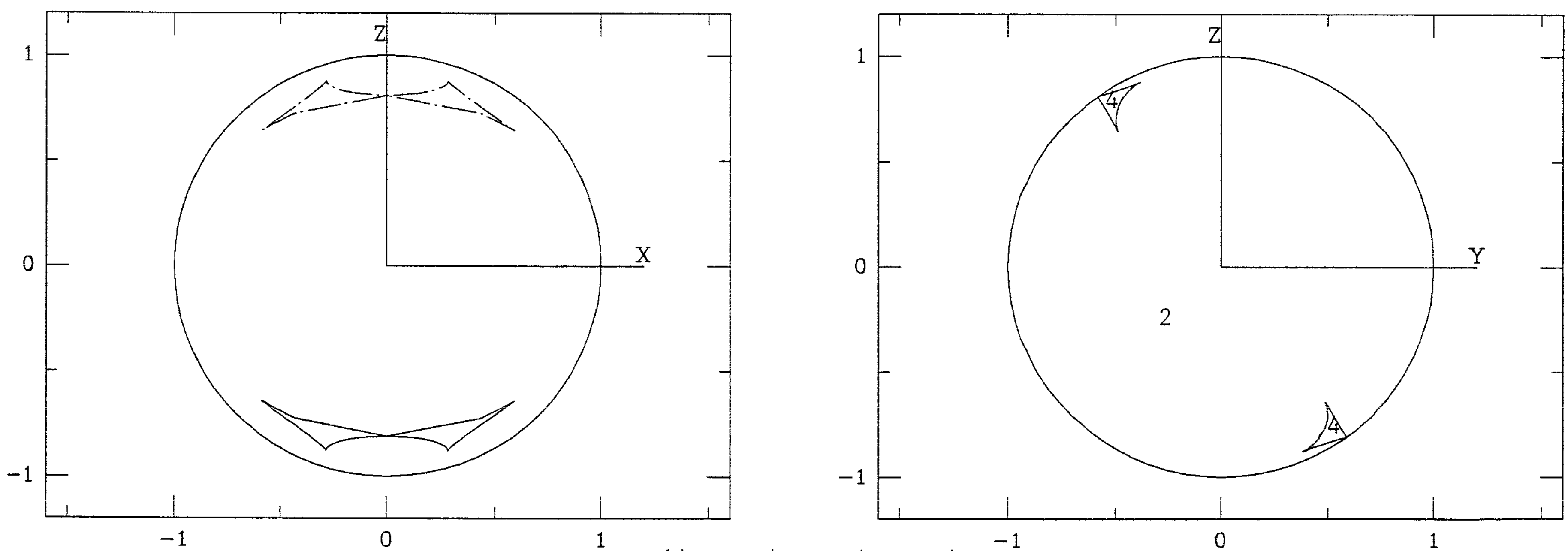

(f) $\alpha_1=\pi/2, \alpha_2=\pi/5, \alpha_3=\pi/2$

Figure 8 (Continued)

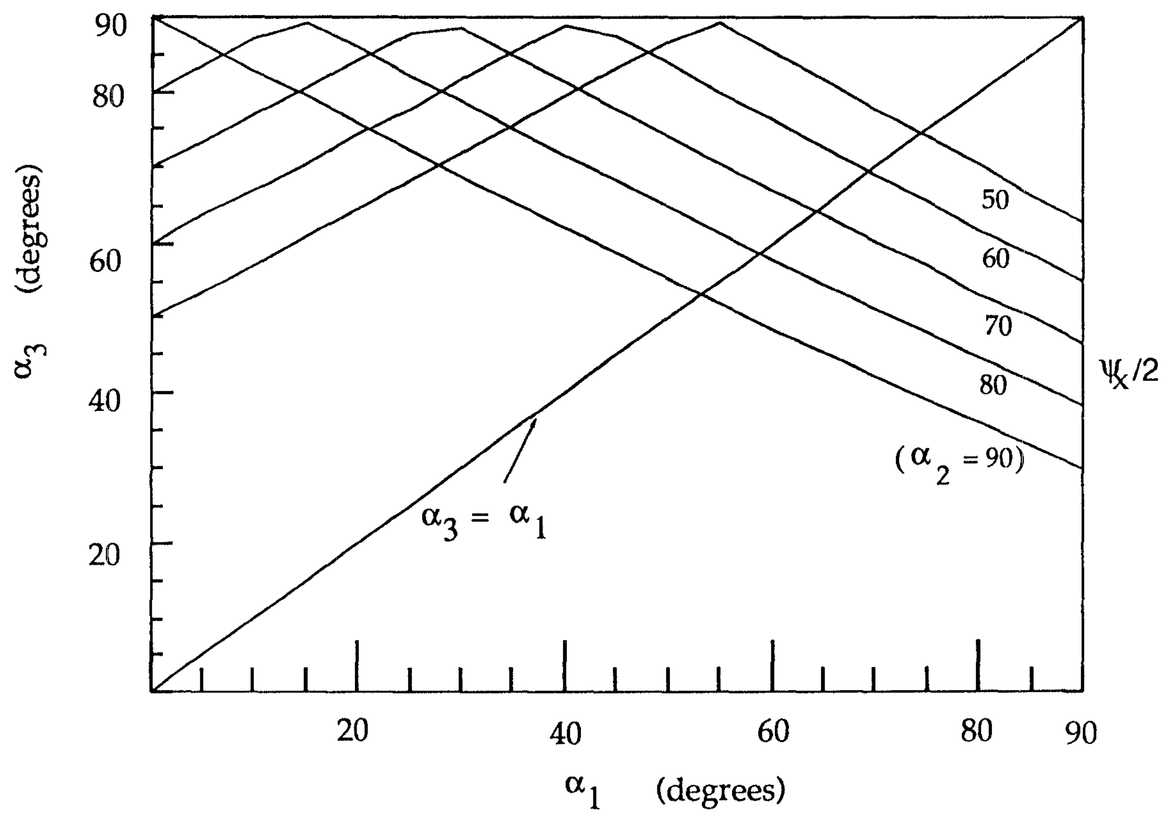

90
80
60
40
20
α_3 (degrees)
20
40
60
80
90
α_1 (degrees)
50
60
70
80
$\psi_x/2$
$(\alpha_2 = 90)$
$\alpha_3 = \alpha_1$

Figure 9